5.4 CERES Edition 3 Cloud Retrievals

Patrick Minnis[1], Sunny Sun-Mack[2], Qing. Z. Trepte[2], Fu-Lung Chang[2], Patrick W. Heck[3], Yan Chen[2], Yuhong Yi[2], Robert F. Arduini[2], Kirk Ayers[2], Kristopher Bedka[2], Sarah Bedka[2], Ricky Brown[2], Sharon Gibson[2], Elizabeth Heckert[2], Gang Hong[2], Zhonghai Jin[2], Rabindra Palikonda[2], Rita Smith[2], William L. Smith, Jr.[1], Douglas A. Spangenberg[2], Ping Yang[4], Christopher R. Yost[2], Yu Xie[4]

[1]NASA Langley Research Center, Hampton, VA, USA
[2]SSAI, Hampton, VA, USA
[3]CIMSS, Madison, WI, USA
[4]Texas A&M University, College Station, TX, USA

1. INTRODUCTION

The Clouds and the Earth's Radiant Energy System (CERES) Project has developed an 10-year dataset of shortwave and broadband flux measurements matched with cloud properties retrieved from TRMM Visible and Infrared Scanner and the MODerate-resolution Imaging Spectroradiometer (MODIS) spectral radiances. These unique datasets, based on the CERES Edition-2 algorithms, have proven quite valuable for studying the role of clouds in climate and for improving and evaluating climate model simulations of clouds and radiation. With the availability of many other datasets, especially from surface-based and satellite-borne active sensors, it has become possible to improve and enhance the cloud retrieval algorithms to provide more accurate characterizations of the cloud 3-D structure and microphysical properties.

This paper briefly describes many of the changes in the CERES cloud algorithms and compares and contrasts the results with those from Edition 2 (Ed2), the original 10-year CERES dataset. This new product from CERES will significantly enhance our understanding of the relationships between clouds and the Earth's radiation budget as well as provide the basis for a reliable record that will extend far beyond the initial 10 years of CERES data.

2. DATA

This study uses *Terra* and *Aqua* MODIS data from 2004, 2006, and 2007. The CERES results are compared with cloud fractions from the International Satellite Cloud Climatology Project (ISCCP; Rossow and Schiffer, 1999), the CALIPSO Version 2 Vertical Feature Mask (Vaughan et al., 2007), and the averaged MODIS Atmosphere Science Team (MAST) cloud amounts from *Terra* (MOD08) and *Aqua* (MYD08) determined using the updated method of Ackerman et al. (1998). The CERES Ed2 methods for detecting clouds and retrieving their properties are described by Minnis et al. (2008a) and Trepte et al. (2003), and Minnis et al. (2010a,b), respectively. CALIPSO and CloudSat (Stephens et al., 2008; Tanelli et al., 2008) cloud and aerosol profile data were matched with MODIS and CERES data by Kato et al. (2010) to produce the CCCM dataset to facilitate synergistic analyses of the clouds.

**Corresponding author address:*
Patrick Minnis, MS 420 NASA Langley Res. Ctr.,
Hampton, VA 23681
E-mail: Patrick.Minnis-1@nasa.gov

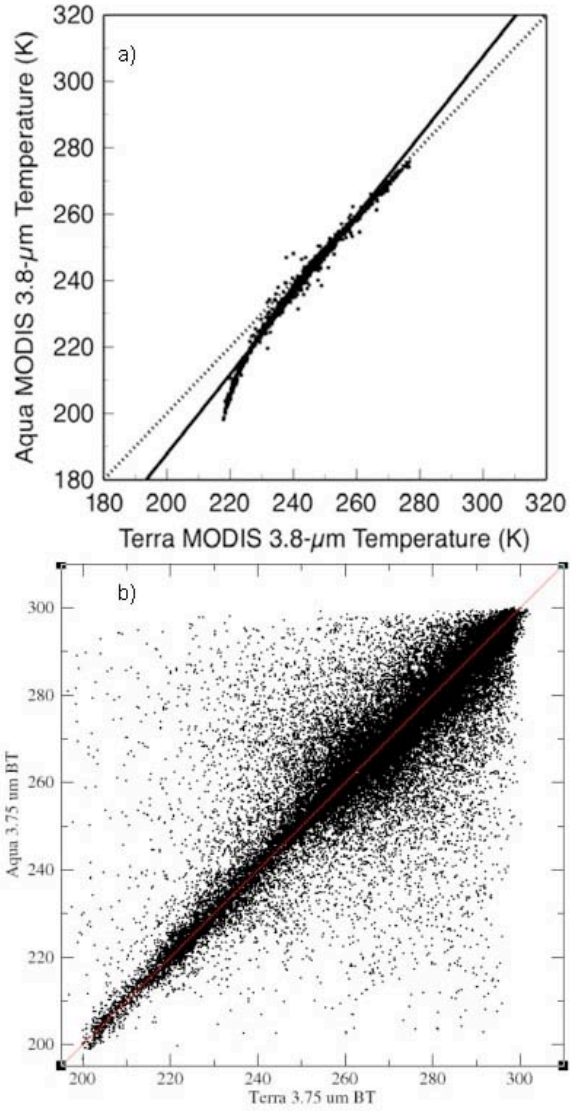

Fig. 1. Scatterplot of nocturnal Terra and Aqua 3.8-μm brightness temperatures. (a) temporally and spatially matched, August 2004 (from Minnis et al. 2008) and (b) averaged over 10' regions, 5 June 2007 after applying correction to Terra.

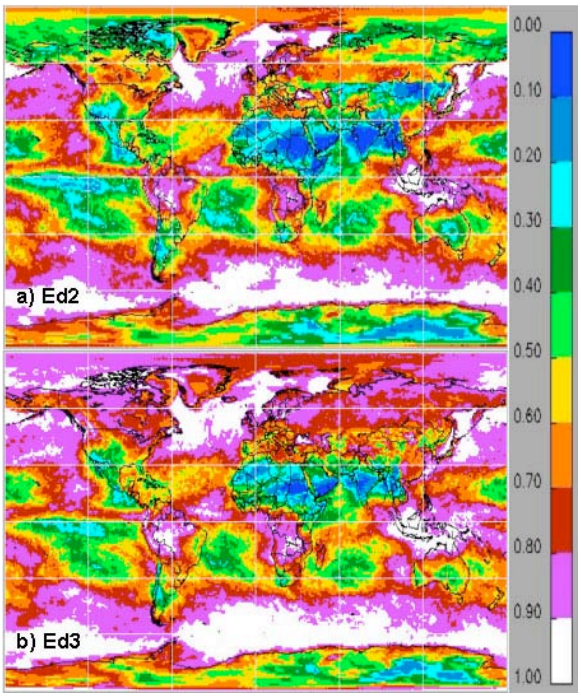

Fig. 2. Average cloud fraction from Terra MODIS data using CERES cloud mask, January 2006.

3. ALGORITHM & DATA CHANGES

Calibration

To obtain a consistent and complementary cloud property dataset from both Terra and Aqua MODIS radiances, the input data should be as consistent as possible. Minnis et al. (2008b) found that the 0.64-μm channel radiances from Terra are 1 – 2% less than those from Aqua, a discrepancy that will introduce differences in retrieved cloud optical depths, τ. The Collection-5 Terra solar channels also appear to have a degradation or discontinuous changes over time that is not seen in the Aqua data. Thus, CERES Edition3 (Ed3) will use the Aqua 0.64-μm channel as a reference and will normalize the Terra calibration to obtain equivalent Aqua radiances using the approach of Minnis et al. (2002), unless MODIS Collection 6 radiance data resolve the differences and are available by the end of 2010. An increase in τ(Terra) is expected.

Minnis et al. (2008a) found that the Collection-5 Terra 3.8-μm brightness temperatures T were ~0.55 K greater than their Aqua counterparts during the daytime and were much greater than those from Aqua at very low temperatures. Figure 1a shows the temporally, angularly, and spatially matched Aqua and Terra averages of T for 0.25° regions during August 2004 (Fig. 2b from Minnis et al., 2008a). The Terra temperatures decrease rapidly from ~255 K to a minimum of ~218 K, while the Aqua values continue to ~195 K. This discrepancy has implications for the cloud mask and retrievals over polar regions. To normalize Terra to Aqua, 0.55 K is subtracted from $T_{3.8}$(Terra) during daylight and for nighttime values exceeding 260 K. A third-order polynomial fit is applied for lower temperatures at night. This correction scheme was applied to Terra data taken during 5 June 2007 and compared to Aqua temperatures taken over the same regions during the same day. Figure 1b shows the scatterplot, which indicates that $T_{3.8}$(Terra), on average, matches $T_{3.8}$(Aqua) quite well over the full range of observations. The large scatter comes from the changes in cloud fraction and temperature that occurred between the Terra and Aqua overpasses. Overall, this change will tend to increase the Terra cloud effective particle size during the day and will alter its cloud mask over polar regions during the night.

Cloud Mask Changes

Minnis et al. (2008) determined that the CERES Ed2 cloud fractions were are roughly 0.06 less than other passive satellite cloud climatologies. The largest differences were found over trade cumulus areas in the tropics. To improve the detection of small cumulus elements, a refined visible-channel threshold and a more sophisticated model of clear ocean reflectance (Jin et al., 2007) were introduced. Also, coding errors in the clear-sky radiance calculations for polar regions were fixed. These and other improvements reported by Trepte et al. (2010) led to increased cloud cover being detected with the preliminary CERES Ed3 algorithms.

Figure 2 compares the mean Ed2 and Ed3 cloud cover from Terra MODIS for January 2006. Cloud cover increased over most locations, especially in the Arctic. Trepte et al. (2010) discuss the apparent overestimation of cloudiness in the proto-Ed3 mask and will be refining the thresholds, especially those relying on the recalibrated 3.8-μm channel. The 2004 seasonal month Ed3 and Ed2 Terra zonal means are plotted in Fig. 3 along with the average cloud amounts from ISCCP and MOD08. The Ed3 averages tend to be slightly larger than those from ISCCP and less than those from MOD08, except for the polar night in the Arctic.

The cloud amount differences are shown more clearly in Fig. 4, which plots the monthly means from the same sources along with the CALIPSO V2 cloud amounts. Results from Aqua are also included. The ISCCP data are for the period 1984 – 2007, while the CALIPSO means are for 2007 - 2008. The MOD08 (MODIS_ST_TER) and MYD08 (MODIS_ST_AQU) are for 2001 - 2009 and 2003 - 2009, respectively. The CERES Terra and Aqua Ed2 results are for 2000 - 2007 and 2002 – 2007, respectively. The CERES Ed3 Aqua data are for 2007 only. The global interannual variability is quite small so these results should be typical. The annual cycles are similar but have some notable differences. The CALIPSO data peak around May and November while the MODIS-ST maxima occur July and November. The ISCCP data have a November maximum but no midyear peak. The CERES Ed2 results have a broad peak from May through August and a November maximum. The CERES Ed3 clouds have a maximum in June with a broad peak from October through January, most likely as a result of the polar night overestimate noted earlier.

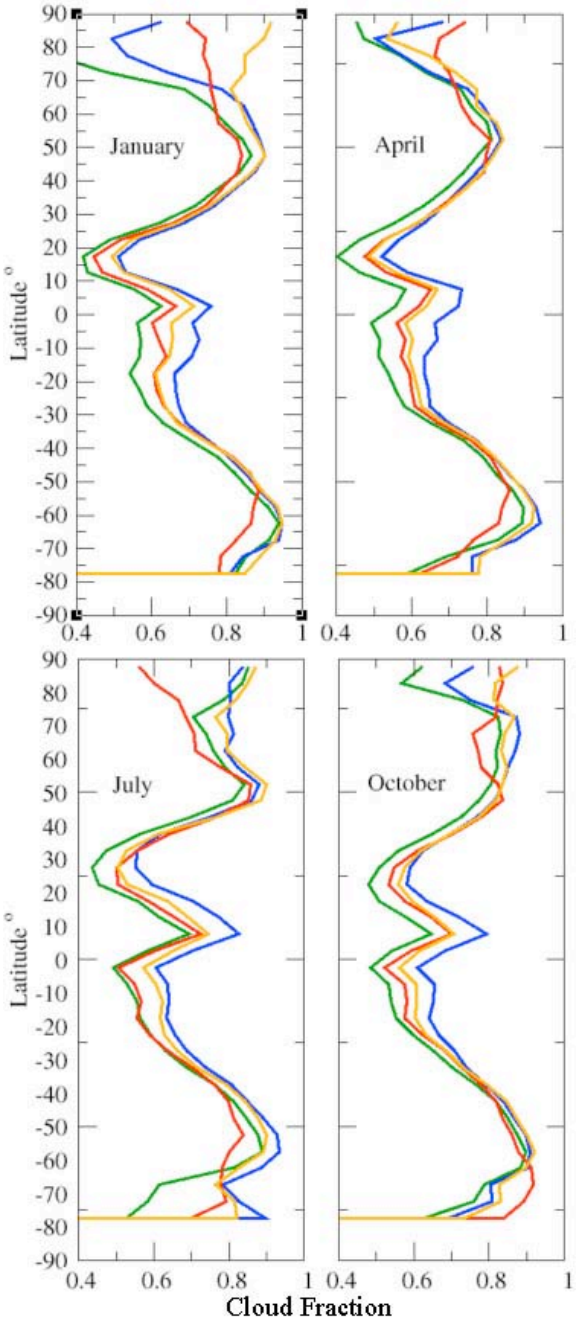

Fig. 3. Monthly mean, 2004 zonal cloud amounts from ISCCP D1 (red) and Terra MODIS data: MOD08 (blue), CERES Ed2 (green), and CERES Ed3 (orange).

The CERES mean cloud cover rose from 0.65 to 0.71 with the new Ed3 algorithm, but is still ~0.05 less than CALIPSO and 0.02 less than the MODIS_ST averages. The Ed3 means are ~0.02 greater than the ISCCP values. Additional refinement of the cloud mask is underway.

Cloud Vertical Structure

The Ed2 cloud top heights Z_t are generally within 0.5 km for single-layer low clouds (e.g., Minnis et al., 2010b), but are typically underestimated by several km for higher clouds, and are ill-defined for multi-layer

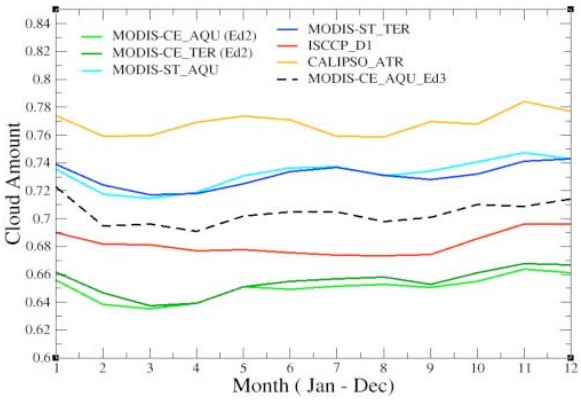

Fig. 4. Monthly mean global cloud fraction over ocean for various time periods.

cloud systems. Several enhancements are introduced in Ed3 to further improve the representation of cloud-top heights. The boundary-layer lapse rate, Γ = -7.1 Kkm^{-1}, used to modify the boundary layer soundings in Ed2 (Minnis et al., 2010a) resulted in some regional low-cloud Z_t biases. A set of regionally dependent mean boundary-layer lapse rates, developed by Sun-Mack et al. (2010) from the CCCM data, provide a means to reduce such regional biases. Figure 5 shows the variation of Γ during the boreal summer. The magnitudes of the ocean values (Fig. 5a) are generally greater than their land counterparts (Fig. 5b). They increase from ~5 Kkm^{-1} near the coasts of the subtropical stratocumulus areas to almost 9 Kkm^{-1} over the Southern Hemisphere storm tracks near 60°S. Over land, the lapse rate magnitudes are smallest, Γ < 5 K km^{-1}, over deserts, and rise to almost 7 Kkm^{-1} over the Arctic. While those variations will not affect the overall mean low cloud heights much, they should yield more accurate regional values.

To improve cloud top height estimates, several changes have been instituted. A new ice crystal reflectance model based on distributions of either roughened hexagonal columns (Yang et al., 2008) or hexagonal columns with imbedded bubbles (Xie et al., 2009) will be used instead of the solid hexagonal column distributions employed in Ed2. These models typically have smaller asymmetry factors resulting in reduced optical depths. This will cause an increase in the retrieved effective heights Z_c for ice clouds having τ < 3. The modified CO_2-absorption technique (MCO2AT) described by Chang et al. (2010a) will provide an independent estimate of cloud pressure p_{co2}. If it is more than 100 hPa less than that the effective cloud pressure p_c determined from the Visible Infrared Shortwave-infrared Split-window Technique (VISST) used in the standard retrievals for clouds having τ < 3, the effective temperature T_c, Z_c, and p_c will be adjusted to match p_{co2}. The optical depth will be altered accordingly to obtain the correct cloud emissivity. For optically thick ice clouds, the values of Z_c and Z_t are nearly equal for Ed2. Ed3 uses the empirical relationship between the two quantities developed by Minnis et al. (2008b) to explicitly determine Z_t from Z_c. In many cases, the differences between the two parameters is 1 – 2 km.

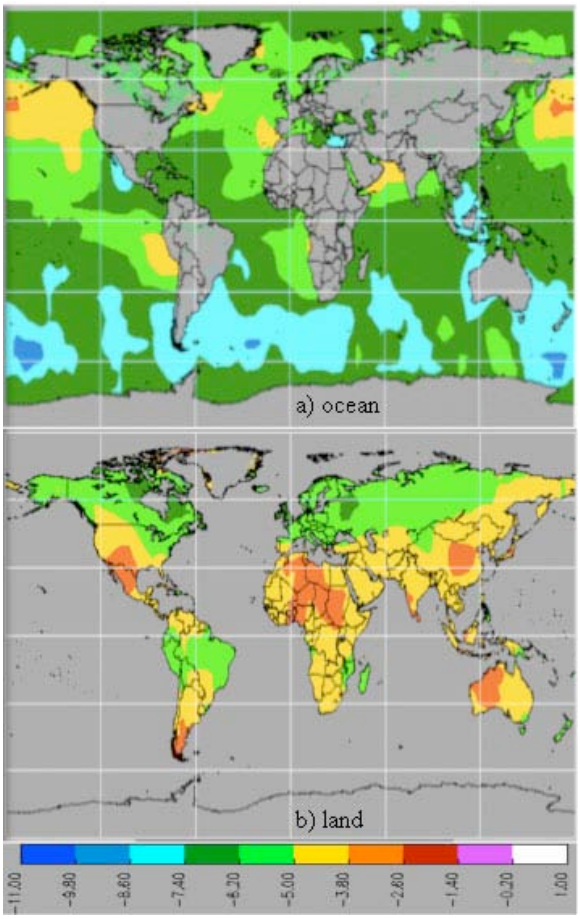

Fig. 5. Daytime boundary-layer lapse rates based on matched CALIPSO and CERES-MODIS cloud-top data, July, August 2006 and June 2006.

To provide a better depiction of cloud vertical structure, the algorithm of Chang et al. (2010b) will be used to detect multilayer clouds that consist of a high ice cloud over low water cloud. Typically the upper-level cloud must have $\tau < 3$ to confidently apply this method. The technique utilizes the MCO2AT to detect the thin high cloud and the VISST-retrieved τ to discriminate between single-layer ice clouds and multilayered clouds. The method explicitly estimates cloud properties separately for the upper and lower layer clouds in each pixel.

The Ed2 analysis uses a set of empirical techniques to estimate cloud physical thickness H so that cloud base height can be computed. Those empirical methods are based on very limited data. To provide more accurate estimates of cloud thickness and base heights, the CCCM data were used to develop new parameterizations using global measurements. The cloud thickness parameterizations were constructed for land and ocean separately for the tropics (20°N – 20°S), the midlatitudes (20°N – 50°N; 20°S – 50°S), and for polar regions (poleward of 50° latitude). For ice clouds,

$$H = H(T_c, \ln\tau, \text{IWP}),$$

while for water clouds,

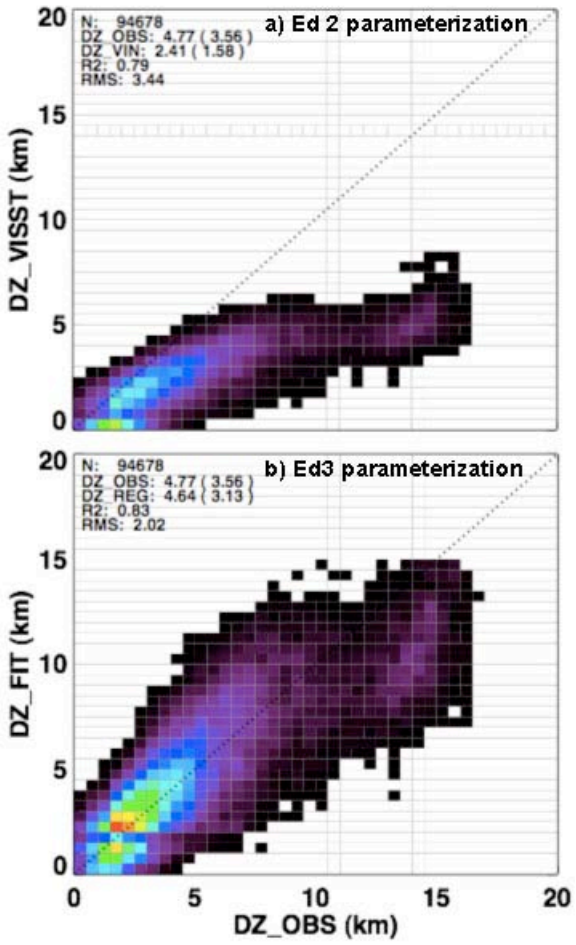

Fig. 6. Comparison of cloud thickness DZ from matched CloudSat-CALIPSO (OBS) and from CERES Aqua MODIS retrievals using Ed2 (VISST) and Ed3 (FIT) parameterizations for ice clouds over tropical oceans, April 2007.

$$H = H(T_c, r_e, \ln\tau, \text{LWP}).$$

In these formulae, r_e is the droplet effective radius, LWP is the liquid water path, and IWP is the ice water path. These equations were determined using several months of CCCM single-layer cloud data. In application, the polar ice cloud parameterization is not used because of poor results in the Aqua Ed2 polar ice cloud retrievals. For Ed3, the midlatitude formula will be used instead. Also, for regions between 20 and 35° of latitude, values of H are computed using both the midlatitude and tropical fits and interpolated linearly. Similarly, interpolation is performed at higher latitudes using the polar and midlatitude water cloud fits.

Figure 6 shows an example of the Ed2 (Fig. 6a) and Ed3 (Fig. 6 b) cloud thicknesses compared to the CCCM CloudSat-CALIPSO values. It clear that the older method dramatically underestimated cloud thickness for most ice clouds. The new method is, on average, unbiased for all $H < 8$, but still has a large uncertainty (~ 2 km) as a result of simplifying the relationships between H and the several variables. While some of the fits are not as accurate as that shown in Fig. 6, the improvement in H for Ed3 is striking for all cloud types.

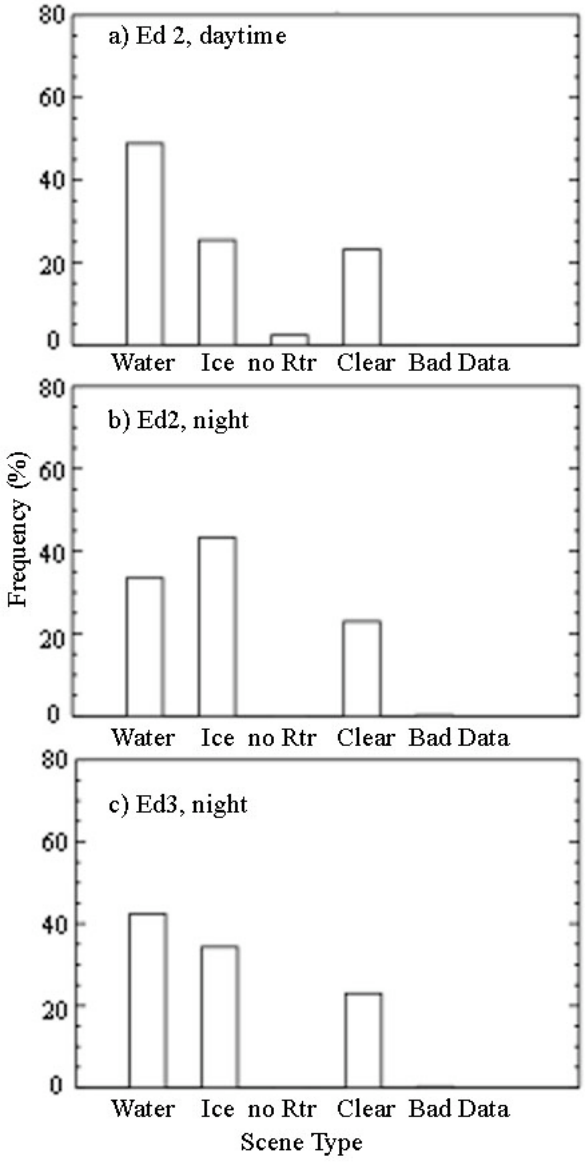

Fig. 7. Pixel classification histograms from CERES analyses of Aqua MODIS data, April and December 2007.

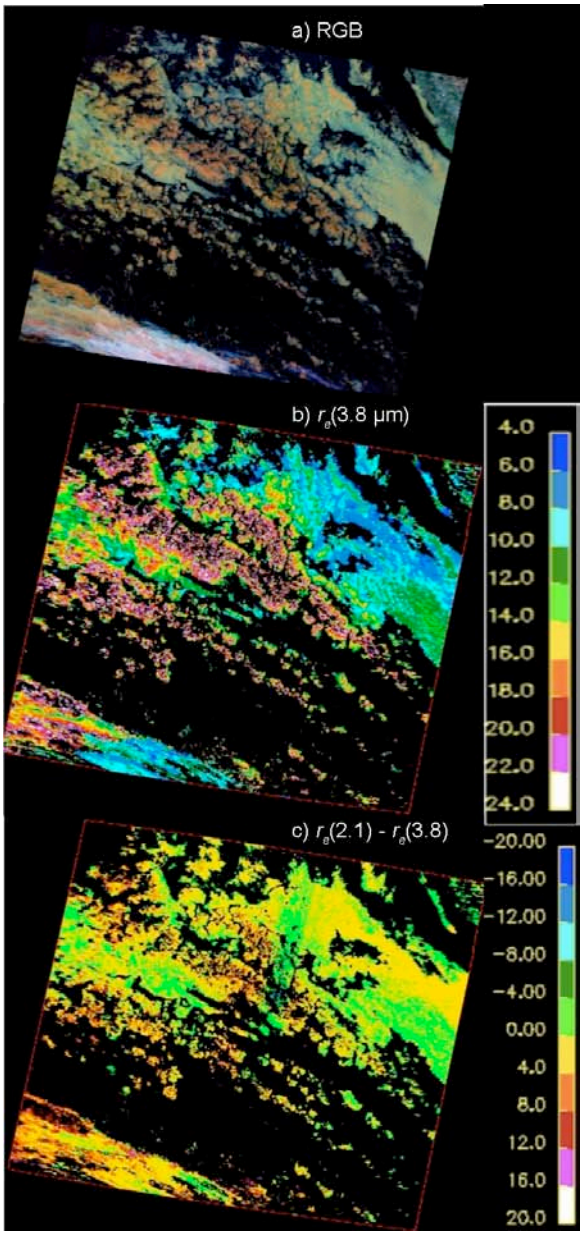

Fig. 8. Example of stratocumulus cloud droplet effective radii derived from (a) Aqua MODIS data using (b) 3.8 μm radiances, and (c) difference between the effective radii retrieved using the MODIS 2.1 and 3.8 μm data.

Cloud Phase

There is a dramatic difference in the Ed2 cloud thermodynamic phase partitioning between daytime and nighttime retrievals, primarily due to the reduced information content resulting from the lack of the 0.64-μm channel at night. The Ed2 algorithms were originally designed to be compatible with the channels available on the TRMM VIRS instrument, so only the 3.8, 10.8, and 12.0-μm channels were used in the retrievals. Since CERES lasted only a short time on the TRMM satellite, the Ed3 algorithms are now permitted to exploit information in other MODIS channels, hence the use of the 13.3-μm channel for the MCO2AT.

To improve the nocturnal phase classification, the 8.5-μm channel is employed in the bispectral method (BSM) of Menzel and Strabala (2002) to provide a first guess for pixels having T_c in the supercooled cloud temperature range (0 to -40°C). The BSM determines the cloud phase as liquid, ice, or mixed. The last category can either be mixed phase or the spectral characteristics of the radiances are too ambiguous for classification with that method. For pixels with T_c in the supercooled range, the phase from the CERES nighttime retrieval algorithm is compared with that from the BSM. If they differ, the BSM phase is selected, unless it is "mixed."

For the mixed clouds, the phase is selected based on how the $BTD_{3.8\text{-}11}$ and $BTD_{11\text{-}12}$ pairs for each pixel compare to linear fits of scatterplots for the same types of pairs accumulated for pixels having definite phase classifications. Figure 7 shows the daytime and night-

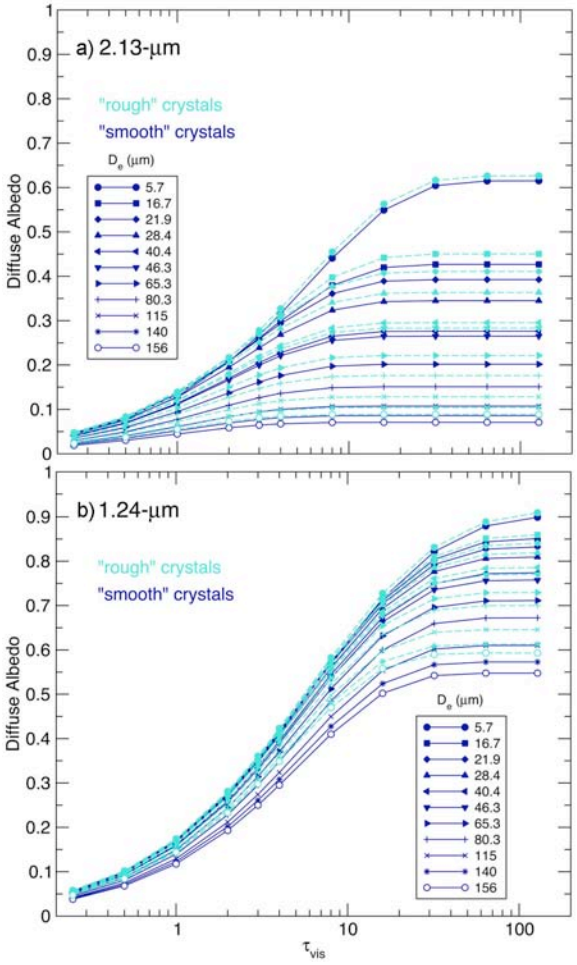

Fig. 9. Cloud diffuse albedos for hexagonal column ice crystal distributions computed using an adding-doubling radiative transfer model.

time histograms of cloud phase for two months of Aqua data. The Ed2 nighttime ice phase fraction (Fig. 7b) occurs 10% more frequently than the water phase, while during the daytime (Fig. 7a), ice clouds are 25% less frequent than the liquid water clouds. Preliminary results from the new nighttime phase algorithm (Fig. 7c) are more consistent with, but not the same as the daytime results. Some of the remaining discrepancy may be to different samplings of ice clouds, actual diurnal differences, and to better detection of thin upper layer ice clouds with the MCO2AT.

Cloud Microphysics

The Ed3 processing also includes retrievals of cloud effective particle size at 1.6 and 2.13 µm in addition to the standard retrieval based on the 3.8-µm channel. Figure 8 shows an example of retrievals over some marine stratocumulus clouds, which have a wide range of droplet sizes at 3.8 µm (Fig. 8b). The differences between $r_e(2.1)$ and $r_e(3.8)$ in Fig. 8c vary from positive to negative indicating that the droplets in the cloud tops are sometimes greater than and other times less than those further down in the cloud. Results like these provide information about cloud water vertical distribution and drizzle.

Other changes in the code include the use of more accurate atmospheric corrections for water vapor absorption, ozone absorption, and Rayleigh scattering that overall tend to decrease the retrieved optical depths by a few percent. The maximum value of τ has been raised to 150, so larger values of IWP and LWP are possible also. The new ice crystal models will have only a small impact on the retrieved values of IWP, but will likely decrease τ and increase the ice crystal effective radius R_e. This latter parameter is the same as the effective diameter D_e used in the Ed2 retrievals, but has been adjusted so that its definition is consistent with other retrievals of ice crystal effective radius (e.g, MOD06). The conversion is as follows.

$$R_e = (7.92 \times 10^{-10}\, D_e^2 + 0.001001\, D_e + 0.4441) * D_e.$$

Over snow-covered areas, Ed3 will likely use the 1.24-µm channel instead of the 2.13-µm channel for retrieving the optical depth because the possible optical depth range can be quite small at 2.13 µm. Figure 9 shows the diffuse albedos at 2.13 and 1.24 µm for different values of τ and D_e. In this instance, $D_e = 2\, R_e$. The albedos become nearly monotonic for many of the models for $\tau < 10$ at 2.13 µm (Fig. 9a). This loss of information occurs for much larger optical depths at 1.24 µm (Fig. 9b). Testing with these models using the clear-sky 1.24-µm albedos derived by Chen et al. (2010) is underway, but will likely confirm that the change to 1.24 µm will be the best route for future retrievals over snow.

Data Availability

It has been difficult to access the CERES cloud data outside of the Single Scanner Footprint data product. To provide more accessibility, an interactive system has been developed to allow users direct access to the various cloud products including monthly and seasonal averages in a variety of forms. Figure 10 shows an example of the interface menu that will be available when Ed3 processing begins.

4. CONCLUDING REMARKS

The new CERES Ed3 products will provide a much more accurate and consistent dataset for climate studies than the previous edition. It should also increase the accuracy of the CERES radiation data in the long run after changes are made in the interpretation of the data for inverting the CERES radiances. The first Ed3 products should be available early in 2011.

5. REFERENCES

Ackerman, S. A., and co-authors, 1998: Discriminating clear sky from clouds with MODIS. *J. Geophys. Res.*, **103**, 32 141–32 157

Bedka, K., and co-authors, 2010: Objective satellite-based detection of overshooting tops using infrared window channel brightness temperature gradients. *J. Appl. Meteorol. Climatol.*, **49**, 181-202.

Chang, F.-L., et al., 2010a: A modified method for inferring upper troposphere cloud top height using the GOES 12 imager 10.7 and 13.3 µm data, *J. Geophys. Res.*, 115, D06208, doi:10.1029/2009JD012304.

Chang, F.-L., P. Minnis, S. Sun-Mack, L. Nyugen, and Yan Chen, 2010: On the satellite determination of multi-layered multi-phase cloud properties. *Proc. AMS 13th Conf. Atmos.*

Rad. and Cloud Phys., Portland, OR, June 27 – July 2, JP1.10.

Chen, Y., P. Minnis, S. Sun-Mack, R. F. Arduini, and Q. Z. Trepte, 2010: Clear-sky and surface narrowband albedo datasets derived from MODIS data. *Proc. AMS 13th Conf. Atmos. Rad. and Cloud Phys.*, Portland, OR, June 27 – July 2, JP1.2.

Jin, Z. H., T. P. Charlock, W. L. Smith, and K. Rutledge, 2004: A parameterization of ocean surface albedo. *Geophys. Res. Lett.*, **31**, L22301, doi:10.1029/2004GL021180

Kato, S., and coauthors, 2010: Relation of cloud occurrence frequency, overlap, and effective thickness derived from CALIPSO and CloudSat merged cloud vertical profiles. *J. Geophys. Res.*, **115**, D00H28, doi:10.1029/2009JD012234.

Menzel, W. P., and K. I. Strabala, 2002: Cloud Top Properties and Cloud Phase - Algorithm Theoretical Basis Document. *Products: 06_L2 (CT). ATBD Reference Number: ATBD-MOD-04.*

Minnis, P., D. R. Doelling, L. Nguyen, W. F. Miller, and V. Chakrapani, 2008b: Assessment of the visible channel calibrations of the TRMM VIRS and MODIS on *Aqua* and *Terra*. *J. Atmos. Oceanic Technol.*, **25**, 385-400.

Minnis, P., and co-authors, 2002: Rapid calibration of operational and research meteorological satellite imagers, Part I: Evaluation of research satellite visible channels as references. *J. Atmos. Oceanic Technol.*, **19**, 1233-1249.

Minnis, P., et al., 2008a: Cloud detection in non-polar regions for CERES using TRMM VIRS and Terra and Aqua MODIS data. *IEEE Trans. Geosci. Rem. Sens.*, **46**, 3857-3884

Minnis, P., and Co-authors, 2010a: CERES Edition-2 cloud property retrievals using TRMM VIRS and Terra and Aqua MODIS data, Part I: Algorithms. Submitted to *IEEE Trans. Geosci. Remote Sens.*

Minnis, P., and co-authors, 2010b: CERES Edition-2 cloud property retrievals using TRMM VIRS and Terra and Aqua MODIS data, Part II: Examples of average results and comparisons with other data. Submitted to *IEEE Trans. Geosci. Remote Sens.*

Minnis, P., C. R. Yost, S. Sun-Mack, and Y. Chen, 2008b: Estimating the physical top altitude of optically thick ice clouds from thermal infrared satellite observations using CALIPSO data. *Geophys. Res. Lett.*, **35**, L12801, doi:10.1029/2008GL033947.

Rossow, W. B. and R. A. Schiffer, 1999: Advances in understanding clouds from ISCCP. *Bull. Amer. Meteorol. Soc.*, **80**, 2261–2287,

Stephens, G. L., et al. 2008: CloudSat mission: Performance and early science after the first year of operation. *J. Geophys. Res.*, **113**, D00A18, doi:10.1029/2008JD009982.

Sun-Mack, S., B. A. Wielicki, P. Minnis, S. Gibson, and Y. Chen, 2007: Integrated cloud-aerosol-radiation product using CERES, MODIS, CALISPO, and CloudSat data. *Proc. SPIE Europe 2007 Conf. Remote Sens. Clouds and the Atmos.*, Florence, Italy, 17-19 September, **6745**, no. 29.

Tanelli, S., and coauthors 2008: CloudSat's cloud profiling radar after two years in orbit: Performance, calibration, and processing. *IEEE Trans. Geosci. Remote Sens.*, **46**, 3560–3573.

Trepte, Q. Z., P. Minnis, C. R. Trepte, S. Sun-Mack, and R. Brown, 2010: Improved cloud detection in CERES Edition 3 algorithm and comparison with the CALIPSO Vertical Feature Mask. *Proc. AMS 13th Conf. Atmos. Rad. and Cloud Phys.*, Portland, OR, June 27 – July 2, JP1.32.

Vaughan, M., and co-authors, 2004: Fully automated analysis of spacebased lidar data: an overview of the CALIPSO retrieval algorithms and data products. *Proc. SPIE Int. Soc. Opt. Eng.*, **5575**, 16–30.

Xie, Y., P. Yang, G. W. Kattawar, P. Minnis, and Y. Hu, 2009: Effect of inhomogeneity of ice crystals on retrieving ice cloud optical thickness and particle size. *J. Geophys. Res.*, **114**, D11203, doi:10.1029/2008JD011216.

Yang, P., G. W. Kattawar, G. Hong, P. Minnis, and Y. X. Hu, 2008: Uncertainties associated with the surface texture of ice particles in satellite-based retrieval of cirrus clouds: Part II. Effect of particle surface roughness on retrieved cloud optical thickness and effective particle size. *IEEE Trans. Geosci. Remote Sens.*, **46**, 1948-1957.

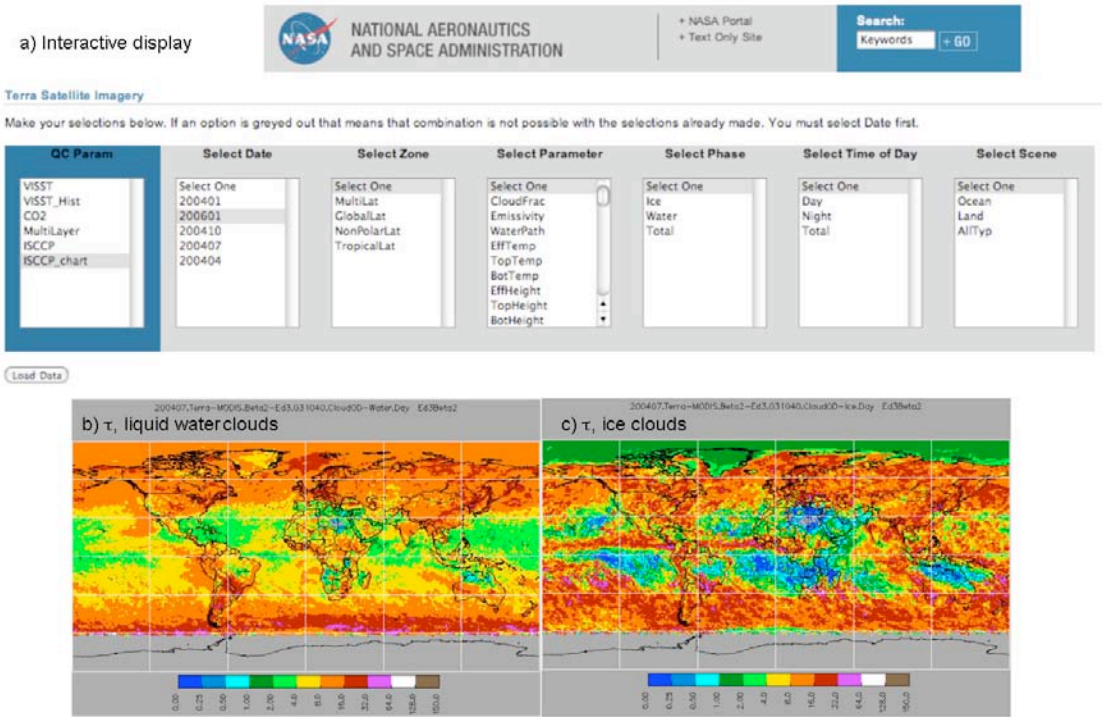

Fig. 10. Interactive web (a) display tool and example, (b) and (c), output images for CERES Ed3 cloud properties.